CMB constraints on the stochastic gravitational-wave background at Mpc scales

Toshiya Namikawa,[1] Shohei Saga,[2] Daisuke Yamauchi,[3] and Atsushi Taruya[2,4]

[1]*Department of Applied Mathematics and Theoretical Physics, University of Cambridge,*
Wilberforce Road, Cambridge CB3 0WA, United Kingdom
[2]*Center for Gravitational Physics, Yukawa Institute for Theoretical Physics,*
Kyoto University, Kyoto 606-8502, Japan
[3]*Faculty of Engineering, Kanagawa University, Kanagawa 221-8686, Japan*
[4]*Kavli Institute for the Physics and Mathematics of the Universe,*
The University of Tokyo Institutes for Advanced Study (UTIAS),
The University of Tokyo, Chiba 277-8583, Japan

We present robust constraints on the stochastic gravitational waves (GWs) at Mpc scales from the cosmic microwave background (CMB) data. CMB constraints on GWs are usually characterized as the tensor-to-scalar ratio, assuming specifically a power-law form of the primordial spectrum, and are obtained from the angular spectra of CMB. Here, we relax the assumption of the power-law form, and consider to what extent one can constrain a monochromatic GW at shorter wavelengths. Previously, such a constraint has been derived at the wavelengths larger than the resolution scale of the CMB measurements, typically above 100 Mpc (below 10^{-16} Hz in frequency). However, GWs whose wavelength is much shorter than 100 Mpc can imprint a small but non-negligible signal on CMB anisotropies at observed angular scales, $\ell < 1000$. Here, using the CMB temperature, polarization, and lensing data set, we obtain the best constraints to date at $10^{-16} - 10^{-14}$ Hz of the GWs produced before the time of decoupling, which are tighter than those derived from the astrometric measurements and upper bounds on extra radiations. In the future, the constraints on GWs at Mpc scales will be further improved by several orders of magnitude with the precision B-mode measurement on large scales, $\ell < 100$.

I. INTRODUCTION

The stochastic gravitational wave (GW) background has been constrained by multiple observations. The cosmic microwave background (CMB) temperature and polarization observations have provided the tightest constraints on the GW background at very low frequencies, $f \lesssim 10^{-16}$ Hz [1–3]. The upper bound on the amplitude of the primordial GW power spectrum has been translated to that on the stochastic GW background at scales larger than the angular resolution of CMB experiments, $k \lesssim 0.1$ Mpc^{-1}, which is equivalent to $f \lesssim 10^{-16}$ Hz in frequency. Combining CMB and LSS data, the GW background is also constrained at higher frequencies, $f = 10^{-16} - 10^{-11}$ Hz, via the upper bound on the extra radiation at the time of CMB decoupling [4–6]. Other astrophysical observations have put constraints on the GW background at roughly the same frequency range. References [7,8] use the motion (astrometry) of quasars and radio sources, respectively, to constrain the GW energy density. Reference [9] derives the constraint on GWs from the secular aberration of the extragalatic radio sources caused by the rotation of the Solar System barycenter around the Galactic center. The stochastic GW background at higher frequencies, $f \gtrsim 10^{-11}$ Hz, is also constrained by

many other direct and indirect observations such as the Pulsar Timing Array [10], big bang nucleosynthesis (BBN) [11], and the Laser Interferometer Gravitational-Wave Observatory (LIGO) [12]. The absence of the primordial black hole also leads to the upper bound on the GW background at a broad range of frequencies [13].

In this paper, we revisit the CMB constraints on the energy density of the stochastic GW background at $k \lesssim 10$ Mpc^{-1} based on the upper bound on the amplitude of the primordial tensor power spectrum. The GW constraints by the primordial tensor power spectrum have been discussed only at the CMB scales, $k \lesssim 0.1$ Mpc^{-1} (see, e.g., [12]). This is because a finite angular resolution of CMB maps limits the observable range of the CMB angular multipole to $\ell \lesssim 1000$, and the observable scale is restricted to $k \simeq \ell/\chi_* \lesssim 0.1$ Mpc^{-1} where $\chi_* \sim 10^4$ is the comoving distance to the CMB last scattering surface. The CMB spectrum is most sensitive to the primordial GWs at $k \lesssim 0.01$ Mpc^{-1} [14]. However, the CMB data can be used to constrain the stochastic GW background at small scales compared to the CMB scale, $k \gtrsim 10$ Mpc^{-1}. The CMB anisotropies and lensing at large-angular scales come from the GW perturbations at low redshifts. Although such contributions are very small, we

find that the upper limits on the large-scale CMB fluctuations provide tighter constraints on the GW energy density at $k = 0.1$–10 Mpc^{-1} than those from other existing constraints at the same scales.

To constrain the energy density of the stochastic GW background using CMB angular spectra, we need to assume a cosmological model for the scalar perturbations, though the degeneracy between the cosmological parameters and GW energy density would be small due to the difference of the angular scale dependence. In this respect, the GW constraints obtained by the CMB angular spectra depend on the model of the scalar perturbations. A less model-independent way to constrain the GW energy density by CMB observations is to use the curl mode of the CMB deflection angle, which has been discussed in several papers [15–18]. In the standard cosmology, the curl mode is consistent with 0 within the current measurement error of Planck. In this paper, we use the curl mode to constrain the GW energy density as a more robust way than using the CMB angular spectra.

This paper is organized as follows. In Sec. II, we begin by discussing the CMB power spectra generated by small-scale GWs, and see their typical behaviors at large angular scales. Then, Sec. III describes the data and our method to derive the constraints on small-scale GWs. Section IV presents our main results, i.e., the upper bound on the energy density of stochastic GWs, together with future forecast. Finally, Sec. V summarizes our work.

II. ANGULAR SPECTRUM

CMB experiments observe the CMB temperature, Θ, and Stokes Q/U maps at each pixel on the unit sphere. The Stokes Q/U maps are decomposed into the E/B modes by the parity symmetry [19,20]. We then obtain the angular spectra of the temperature and B modes by squaring the harmonic coefficients of the CMB anisotropies.

The CMB primary anisotropies are distorted by gravitational lensing from the large-scale structure [21,22]. The lensing distortion is described by a remapping of the CMB fluctuations at the CMB last scattering by a deflection angle, $\boldsymbol{d}$. The lensing effect leads to mode couplings between different CMB multipoles [23]. This mode coupling can be used to reconstruct a map of the curl mode of the deflection angle, $\varpi = (\star \nabla) \cdot \boldsymbol{d}$, from an observed CMB map (e.g., [24,25]), where $\star$ is the rotation operator for a two dimensional vector [25]. We then measure the curl-mode spectrum.

Given the initial dimensionless power spectrum of GWs, $\Delta_t(k)$, the CMB and curl-mode spectra are theoretically computed, with a help of the CMB Boltzmann code, as

$$C_\ell^{XX} = 4\pi \int \mathrm{d}\ln k \Delta_t(k)$$
$$\times \int \mathrm{d}\chi j_\ell(k\chi) S^X(k,\chi) \int \mathrm{d}\chi' j_\ell(k\chi') S^X(k,\chi'), \quad (1)$$

with $X = \Theta$, B, or ϖ. In this paper, the source functions, $S^X(k,\chi)$, and angular spectra C_ℓ^{XX} are computed, modifying CAMB [26]. To obtain a generic constraint on stochastic GWs in a rather model-independent manner, we consider a monochromatic GW given at the wave number, k_c. The dimensionless power spectrum of GW is then given by

$$\Delta_t(k) = \begin{cases} A_{\mathrm{GW}}/(2\epsilon) & (|k/k_c - 1| \leq \epsilon) \\ 0 & (\text{otherwise}) \end{cases}. \quad (2)$$

Here, A_{GW} is the amplitude of GW, and ϵ characterizes the width of the GW spectrum in wave number. We divide the wave number between 10^{-4} Mpc$^{-1} \leq k \leq 10$ Mpc^{-1} into logarithmically equal 20 bins. We checked that our result remains unchanged even if we change the bin number to a larger value.

Figure 1 shows the angular spectra of the CMB temperature (left), B mode (middle), and curl mode (right) for various wave numbers k_c. The amplitude of the power spectra is given by $A_{\mathrm{GW}} = rA_s$, where the tensor-to-scalar ratio r is set to be the current best upper bound, $r = 0.06$ [2], with the scalar amplitude at $k = 0.05$ Mpc^{-1} determined by the latest Planck cosmology, $A_s = 2.1 \times 10^{-9}$ [3]. The large-scale Fourier modes ($k_c \ll 1$ Mpc^{-1}) contribute to the power spectrum at large scales. Similarly, the small-scale Fourier modes ($k_c \gg 1$ Mpc^{-1}) mostly generate the small-scale fluctuations. The large-scale fluctuations from such small-scale Fourier modes are typically small but their contribution is not exactly 0.

To elucidate the low-ℓ behaviors shown in Fig. 1, one may compare the exact calculation with the Limber approximation. In the Limber approximation, the source function S^X and power spectrum Δ_t in the integrand of Eq. (1) are assumed to be a smooth function of k. Then, the integral convolving spherical Bessel function over k exhibits a heavy cancellation, which results in a rather simplified form of the angular spectrum (see, e.g., [21,27]);

$$C_\ell^{XX} \simeq \frac{2\pi^2}{\ell^3} \int \mathrm{d}\chi \chi \Delta_t\left(k = \frac{\ell}{\chi}\right)\left[S^X\left(k = \frac{\ell}{\chi}, \chi\right)\right]^2, \quad (3)$$

which tells us that the amplitude of C_ℓ^{XX} is determined by the contribution of GWs at the wave number $k = \ell/\chi$ projected along the line of sight (i.e., χ-integral). Strictly speaking, the above equation is inadequate in our case because the integrand contains the top-hat primordial power spectrum. Further, the tensor transfer function has oscillatory behaviors, which, combining with spherical Bessel function, leads to a rather nontrivial cancellation. Nevertheless, Eq. (3) can be used for a qualitative understanding of the angular spectrum.

In Fig. 2, we specifically set the top-hat GW spectrum to the one centered at $k_c = 0.014$ Mpc^{-1} with the width $\Delta k = 0.008$ Mpc^{-1}, and plot the angular spectra with
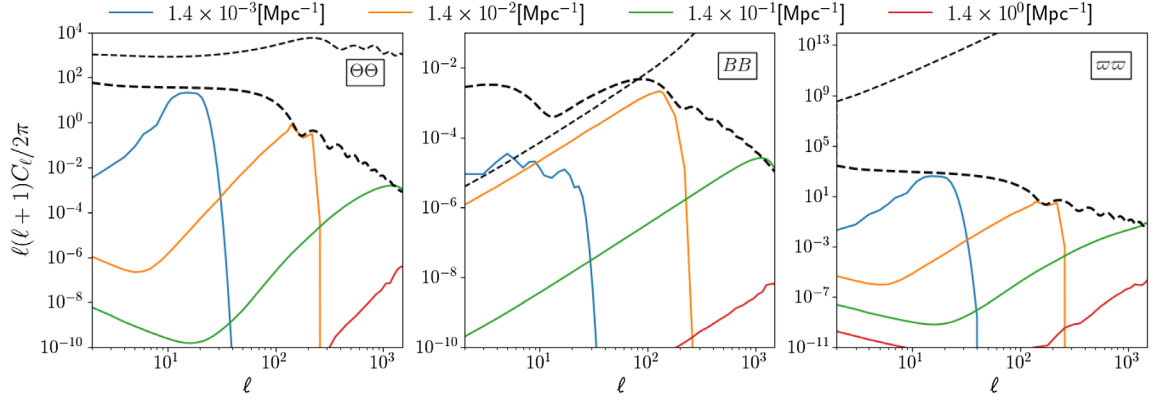
FIG. 1. The angular spectra of the CMB temperature, B mode, and lensing curl mode with varying the central frequency, k_c (solid lines). The amplitude of the power spectra is given by $A_{\mathrm{GW}} = rA_s$ where the tensor-to-scalar ratio is chosen as the current best upper bound, $r = 0.06$ [2], and the scalar amplitude at $k = 0.05$ Mpc^{-1} is consistent with the latest Planck cosmology, $A_s = 2.1 \times 10^{-9}$. The gray dashed lines in the temperature and B-mode spectra show the contributions from the scalar perturbations, while that in the curl-mode spectrum shows the reconstruction noise of the Planck observation. The black dashed lines show the inflationary GW contributions with $r = 0.1$.

and without the Limber approximation. Then, in all cases, the results with Limber approximation exhibit a sharply peaked structure around $\ell_* \equiv k_c\chi_*$, indicated by the two vertical dashed lines, where χ_* is the comoving distance to the last scattering surface of CMB. At higher multipoles of $\ell > \ell_*$, the amplitudes rapidly falls off, consistent with exact calculations. These behaviors basically come from the nature of photon radiative transfer encapsulated in the function S^X. On the other hand, looking at the lower multipoles of $\ell_* < \ell$, while the Limber approximation predicts a rather suppressed B-mode spectrum that fails to reproduce the exact calculation, the predictions of the temperature and curl-mode spectra show a rather long tail, which qualitatively explains the behaviors in the exact calculations. Recall that in the Limber approximation, the top-hat GWs peaked at k_c can contribute to C_ℓ only at the

multipole $\ell = k_c\chi$; Fig. 2 implies that the low-ℓ behaviors of the exact calculation in the temperature and curl-mode spectrum mainly comes from the low-z GW contributions (i.e., $\chi \lesssim \chi_*$), whereas a non-negligible amount of the high-z GWs plays a role to determine the low-ℓ amplitude of the B-mode spectrum.

Having confirmed the typical behaviors of the angular spectra, we further consider the small-scale GWs, and plot in Fig. 3 the angular spectra for $k_c > 1$ Mpc^{-1}. The results are compared with the contributions from the scalar perturbations or the reconstruction noise. As we have seen in Figs. 1 and 2, no appreciable low-ℓ tail is developed for the B-mode spectrum, since the polarization is only generated at the reionization and recombination. Figure 3 suggests that the B-mode constraint on the small-scale GWs is basically limited by the angular resolution of CMB observations.
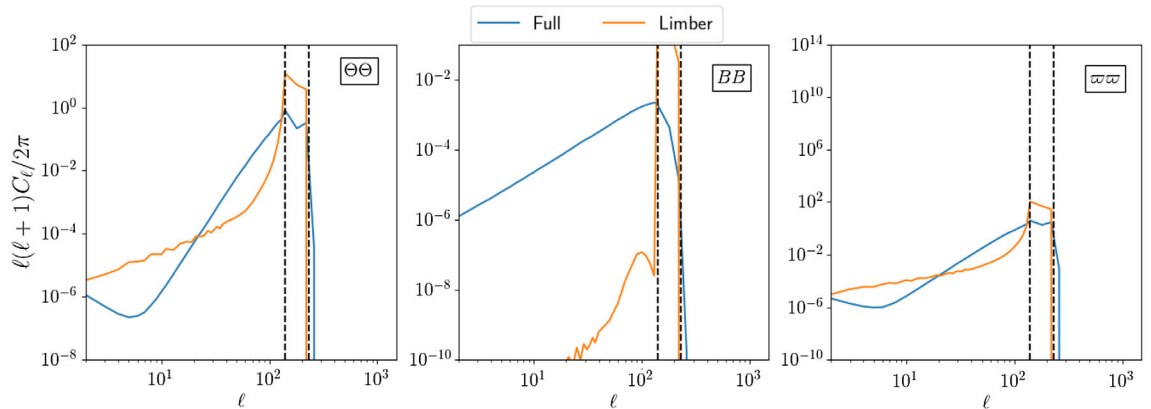

FIG. 2. The angular spectra of the CMB temperature, B mode, and lensing curl mode from a top-hat primordial GW power spectrum with 0.01 Mpc$^{-1} \leq k \leq 0.018$ Mpc^{-1} using the Limber approximation, $\ell = k\chi$. The amplitude of the power spectra is the same as that in Fig. 1. The vertical dashed lines show $\ell = 0.01\chi_*$ Mpc^{-1} and $\ell = 0.018\chi_*$ Mpc^{-1}. For comparison, we also show the results without the Limber approximation (blue).
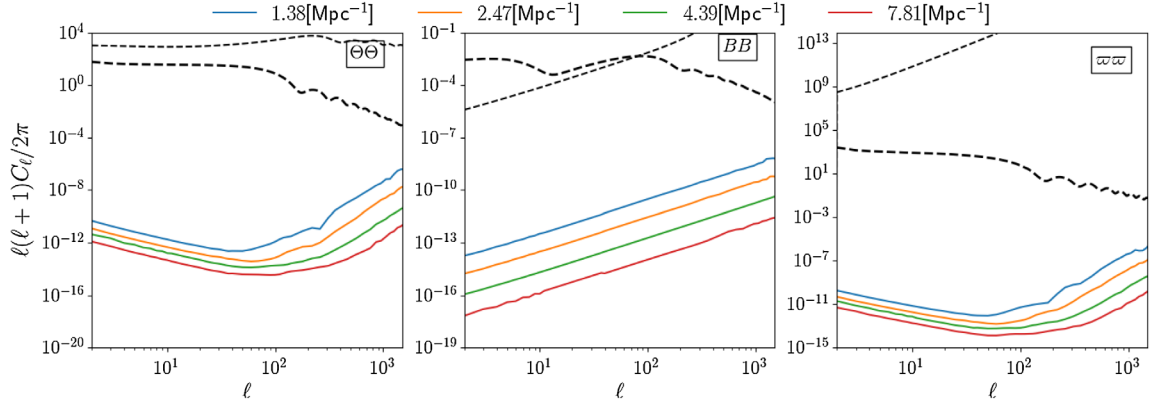
FIG. 3.   Same as Fig. 1 but for $k_c > 1 \text{ Mpc}^{-1}$.

On the other hand, the temperature and curl-mode power spectra exhibit a low-ℓ tail that is more prominent and is rather enhanced compared to the results in Fig. 1. This implies that large angle CMB data can still give a meaningful constraint on small-scale GWs.

III. DATA AND METHOD

Here, we explain the data and the analysis method to constrain the stochastic GWs, particularly paying attention at small scales. In our analysis, we use the CMB temperature spectrum, $C_\ell^{\Theta\Theta}$, measured by Planck [3], the B-mode spectrum, C_ℓ^{BB}, by BICEP/Keck Array [2], and curl-mode spectrum, $C_L^{\varpi\varpi}$, by Planck [28]. Note that the constraints from the temperature-E cross and E-mode autospectra measured by Planck turn out to be statistically insignificant compared to that obtained by the temperature spectrum. In this paper, therefore, we only present the results from the temperature, B-mode, and curl-mode spectra. We checked that our constraints remain unchanged even if we add other B-mode spectra measured by POLARBEAR [29] and SPTpol [30].

Provided the data, the constraint on the amplitude of stochastic GW, A_{GW}, assuming the monochromatic wave with wave number k_c, is obtained by minimizing the likelihood function $\mathcal{L}$. We adopt here the Gaussian likelihood function,

$$-2\ln\mathcal{L}(A_{\text{GW}}) = \sum_{b=1}^{n} \frac{[\hat{C}_b^{XY} - C_b^{XY,\text{fid}}(A_{\text{GW}})]^2}{(\sigma_b^{XY})^2}, \quad (4)$$

where the subscript b indicates the index of the multipole bins, and n is the number of the multipole bins. The label XY implies $\Theta\Theta$, BB, or $\varpi\varpi$. The power spectrum $\hat{C}_b^{XY}$ is the measured binned spectrum, and $C_b^{XY,\text{fid}}(A_{\text{GW}})$ is the theoretical prediction having a specific GW amplitude A_{GW}. Finally, σ_b^{XY} is the measurement error of the angular spectrum provided by the CMB experiments described above. The multipole ranges used in the likelihood analysis

are $2 \le \ell \le 2508$ for temperature, $37 \le \ell \le 332$ for B-mode, and $2 \le \ell \le 2020$ for curl-mode spectra, respectively, at which the data are validated.

The observed temperature spectrum has contributions from both the scalar and tensor perturbations. In the B-mode spectrum, the gravitational lensing effect generates the B mode even if there is only the scalar perturbation [31]. Thus, we simultaneously need to model or constrain the non-GW contributions to constrain GWs in the angular spectra. In our analysis, we simply subtract the contributions of the scalar perturbations from the measured spectrum, assuming the Planck best-fit ΛCDM model, since the degeneracy between the GW amplitude and cosmological parameters would be small and does not increase the upper bound by more than an order of magnitude.

The upper bound on A_{GW} obtained from the above analysis is then translated to the GW fractional energy density defined as

$$\Omega_{\text{GW}}(k) \equiv \frac{1}{\rho_c} \frac{d\rho_{\text{GW}}}{d\ln k}\bigg|_{\eta=\eta_0} = \frac{\Delta_t(k)}{12H_0^2}\left(\frac{\partial T(k,\eta_0)}{\partial\eta}\right)^2$$
$$= \frac{(A_{\text{GW}}/2\epsilon)}{12H_0^2}\left(\frac{\partial T(k,\eta_0)}{\partial\eta}\right)^2, \quad (5)$$

at $|k/k_c - 1| \le \epsilon$ and 0 otherwise, where ρ_c is the critical density of the Universe, and H_0 is the Hubble parameter today. The time derivative of the GW transfer function is computed by CAMB assuming no neutrino anisotropic stress [26].

IV. RESULTS

Figure 4 shows the 95% C.L. upper bounds on the GW amplitudes at each scale using the current best measurements of the CMB angular spectra. At $k = 0.01 \text{ Mpc}^{-1}$, the best constraints come from the B-mode spectrum measured by BICEP2/Keck Array. At smaller scales, $k \gtrsim 0.1 \text{ Mpc}^{-1}$, however, the temperature spectrum obtained by Planck provides the constraints on the GW amplitudes comparable
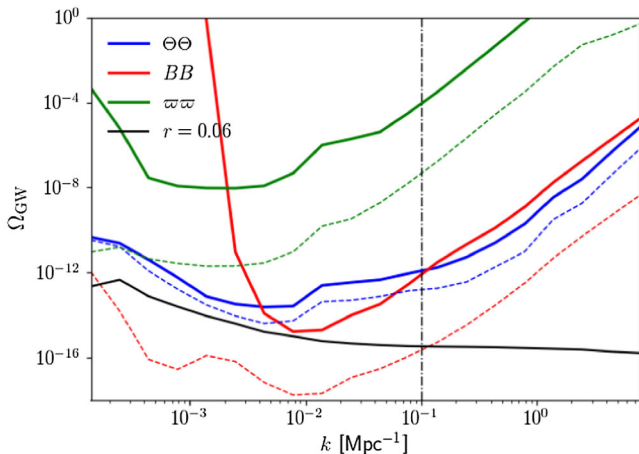
FIG. 4. The current 95% upper bounds on the amplitude of the stochastic GW background at $k < 10$ Mpc^{-1} by the CMB observations. For reference, we show the energy density of the scale-invariant primordial GW with $r = 0.06$ as a function of k (black solid). The dashed lines are the expected upper bounds by a future CMB observation. The vertical dot-dashed line roughly corresponds to the maximum observable wave number determined by the resolution of CMB experiments.

to that from the B-mode spectrum. At large scales, the constraint by the B-mode spectrum becomes very weak because the B-mode spectrum is not measured at $\ell \lesssim 30$.

Figure 4 also plots the expected constraints on the GW spectrum amplitude by future CMB observations. In this forecast, we assume an idealistic future CMB experiment, i.e., a full sky observation, 1 μK-arcmin white noise with 1 arcmin Gaussian beam. We also assume no foregrounds and 90% of the lensing B mode is removed. Thus, the results provide the expected constraints in the most optimistic case. In the future, the constraints from the temperature spectrum are not significantly improved since the current temperature measurement is already dominated by the scalar perturbations at $\ell < 2000$. On the other hand, the B mode and curl mode are still dominated by the instrumental and reconstruction noise, respectively. The constraints are improved if the noise contribution is reduced in the future. The tightest constraints are obtained from the measurement of the B-mode spectrum.

V. SUMMARY AND DISCUSSION

In this paper, using the currently available CMB data, we presented robust constraints on stochastic GWs at Mpc scales, which are far below the resolution limit of CMB measurements. The key point is that even the short-wavelength GWs can still give an impact on the power spectrum of CMB anisotropies at large angular scales, to which we cannot apply the Limber approximation due to the heavily oscillatory behaviors of GWs. Using the available CMB data of temperature, B-mode polarization, and lensing from Planck and BICEP/Keck array, we find that currently both the

temperature and B-mode data put the constraint almost at the same level at $k \gtrsim 0.1$ Mpc^{-1}, summarized as

$$\Omega_{\mathrm{GW}} \lesssim 10^{-12} \left(\frac{k}{0.1 \text{ Mpc}^{-1}} \right)^3, \qquad (6)$$

which is compared with other constraints shown in Fig. 5. Note that Eq. (6), strictly speaking, valid at $k \lesssim 10$ Mpc^{-1}, at which we stop constraining GW due to the heavy oscillations of the spherical Bessel function and source function in the integrand of Eq. (1) However, it is expected from the behaviors seen in Fig. 3 that the scaling given at Eq (6) still holds at $k \gtrsim 10$ Mpc^{-1}, thus giving a meaningful constraint complementary to those coming from astrometric observation and thermal history of the Universe.

In the future, a tighter constraint will be obtained from the B-mode polarization, and the expected constraint will be improved by several orders of magnitude. Note cautiously that the constraints coming from the temperature and B-mode data are model dependent in the sense that the constraints are obtained from the data subtracting the primary (temperature) or secondary (B-mode) signal created by the scalar perturbations, for which we assume ΛCDM model. In this respect, the curl-mode data give complementary information to the temperature and B-mode polarization, although the constraining power is significantly degraded.

Finally, the constraints obtained here are useful in narrowing the parameters of several models that can produce the GWs at Mpc scales. The early universe scenarios producing a blue-tilted stochastic GW are obviously interesting targets to
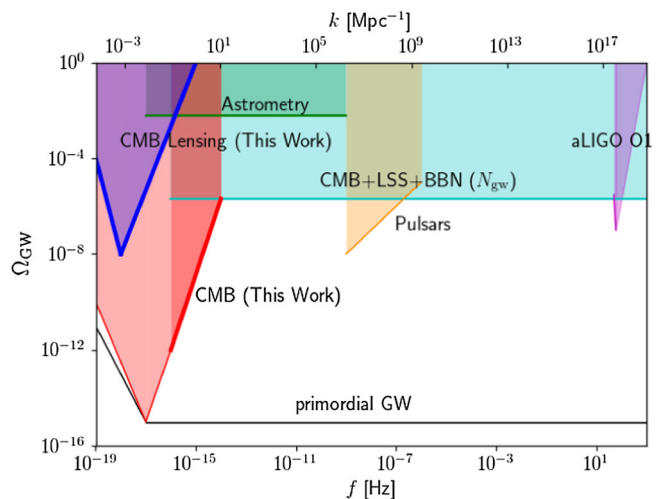

FIG. 5. Summary of the current status of the upper bounds on the energy density of the stochastic GW background. The thick red and blue shaded regions correspond to the constraints obtained in this paper using the CMB angular spectra and curl mode of the gravitational lensing, respectively. We also show other constraints from the astrometry of radio sources (astrometry) [8], extra radiation before CMB decoupling (CMB+ LSS + BBN) [6,32], pulsar Timing (pulsars) [10], and GW interferometers (aLIGO O1) [12].

constrain (e.g., [33]). Apart from these, the constraint on cosmic string models is also worth consideration. The stochastic GW spectrum produced by the cosmic strings depends significantly on the model parameters and assumptions as shown in Refs. [34–36], and thus constraining the GWs over a very broad frequency range is important to pin down the cosmic string models. Another possible source of GWs at Mpc scales is the ultralight axion motivated by string theory. Reference [37] discusses the possibility that the ultralight axion produces a sizable amount of GWs through the nonlinear scalar field interaction induced by parametric resonance, and the produced GWs can have a peak with broad distribution at Mpc scales if the axion mass is around $m \sim 10^{-22}$ eV. This mass scale lies at the scales for which the axion can put an interesting imprint on the small-scale structure [38–42]. Several works also discuss generation of GWs at Mpc scales assuming that the primordial GW power spectrum has a sharp peak [32,43]. The constraint on stochastic GWs obtained in this paper certainly helps to exclude a part of parameter regions that can produce a large GW amplitude, although a detailed analysis is still necessary to get a constraint, using properly the shape of the predicted GW spectrum.

[1] BICEP2 and Planck Collaborations, Joint Analysis of BICEP2/Keck Array and Planck Data, Phys. Rev. Lett. **114,** 101301 (2015).

[2] BICEP2/Keck Array Collaboration, BICEP2/Keck Array X: Constraints on Primoridal Gravitational Waves Using Planck, WMAP, and New BICEP2/Keck Observations through the 2015 Season, Phys. Rev. Lett. **121,** 221301 (2018).

[3] Planck Collaboration, Planck 2018 results. VI. Cosmological parameters, Astron. Astrophys., arXiv:1807.06209.

[4] T. L. Smith, E. Pierpaoli, and M. Kamionkowski, A New Cosmic Microwave Background Constraint to Primordial Gravitational Waves, Phys. Rev. Lett. **97,** 021301 (2006).

[5] T. L. Smith, M. Kamionkowski, and A. Cooray, Direct detection of the inflationary gravitational wave background, Phys. Rev. D **73,** 023504 (2006).

[6] L. Pagano, L. Salvati, and A. Melchiorri, New constraints on primordial gravitational waves from Planck 2015, Phys. Lett. B **760,** 823 (2016).

[7] C. R. Gwinn, T. M. Eubanks, T. Pyne, M. Birkinshaw, and D. N. Matsakis, Quasar proper motions and low frequency gravitational waves, Astrophys. J. **485,** 87 (1997).

[8] J. Darling, A. E. Truebenbach, and J. Paine, Astrometric limits on the stochastic gravitational wave background, Astrophys. J. **861,** 113 (2018).

[9] O. Titov, S. B. Lambert, and A. M. Gontier, VLBI measurement of the secular aberration drift, Astron. Astrophys. **529,** A91 (2011).

[10] P. D. Lasky *et al.*, Gravitational-Wave Cosmology Across 29 Decades in Frequency, Phys. Rev. X **6,** 011035 (2016).

[11] S. Henrot-Versille *et al.*, Improved constraint on the primordial gravitational-wave density using recent cosmological data and its impact on cosmic string models, Classical Quantum Gravity **32,** 045003 (2015).

[12] LIGO Scientific and Virgo Collaborations, Upper Limits on the Stochastic Gravitational-Wave Background from Advanced LIGOs First Observing Run, Phys. Rev. Lett. **118,** 121101 (2017).

[13] T. Nakama and T. Suyama, Primordial black holes as a novel probe of primordial gravitational waves. II: Detailed analysis, Phys. Rev. D **94,** 043507 (2016).

[14] T. Hiramatsu, E. Komatsu, M. Hazumi, and M. Sasaki, Reconstruction of primordial tensor power spectra from B-mode polarization of the cosmic microwave background, Phys. Rev. D **97,** 123511 (2018).

[15] A. Cooray, M. Kamionkowski, and R. R. Caldwell, Cosmic shear of the microwave background: The curl diagnostic, Phys. Rev. D **71,** 123527 (2005).

[16] D. Sarkar, P. Serra, A. Cooray, K. Ichiki, and D. Baumann, Cosmic shear from scalar-induced gravitational waves, Phys. Rev. D **77,** 103515 (2008).

[17] T. Namikawa, D. Yamauchi, and A. Taruya, Future detectability of gravitational-wave induced lensing from high-sensitivity CMB experiments, Phys. Rev. D **91,** 043531 (2015).

[18] S. Saga, D. Yamauchi, and K. Ichiki, Weak lensing induced by second-order vector mode, Phys. Rev. D **92,** 063533 (2015).

[19] M. Kamionkowski, A. Kosowsky, and A. Stebbins, A Probe of Primordial Gravity Waves and Vorticity, Phys. Rev. Lett. **78,** 2058 (1997).

[20] U. Seljak and M. Zaldarriaga, Signature of Gravity Waves in Polarization of the Microwave Background, Phys. Rev. Lett. **78,** 2054 (1997).

[21] A. Lewis and A. Challinor, Weak gravitational lensing of the CMB, Phys. Rep. **429,** 1 (2006).

[22] D. Hanson, A. Challinor, and A. Lewis, Weak lensing of the CMB, Gen. Relativ. Gravit. **42,** 2197 (2010).

[23] D. Hanson and A. Lewis, Estimators for CMB statistical anisotropy, Phys. Rev. D **80,** 063004 (2009).

[24] T. Okamoto and W. Hu, The angular trispectra of CMB temperature and polarization, Phys. Rev. D **66,** 063008 (2002).

[25] T. Namikawa, D. Yamauchi, and A. Taruya, Full-sky lensing reconstruction of gradient and curl modes from CMB maps, J. Cosmol. Astropart. Phys. 01 (2012) 007.

[26] A. Lewis, A. Challinor, and A. Lasenby, Efficient computation of CMB anisotropies in closed FRW models, Astrophys. J. **538,** 473 (2000).

[27] M. Loverde and N. Afshordi, Extended limber approximation, Phys. Rev. D **78,** 123506 (2008).

[28] Planck Collaboration, Planck 2013 results. XVII. Gravitational lensing by large-scale structure, Astron. Astrophys. **571,** A17 (2014).

[29] P. A. R. Ade *et al.* (POLARBEAR Collaboration), A measurement of the cosmic microwave background *B*-mode polarization power spectrum at sub-degree scales from 2 years of POLARBEAR data, Astrophys. J. **848,** 121 (2017).

[30] R. Keisler *et al.* (SPTpol Collaboration), Measurements of sub-degree B-mode polarization in the cosmic microwave background from 100 square degrees of SPTpol data, Astrophys. J. **807,** 151 (2015).

[31] M. Zaldarriaga and U. Seljak, Gravitational lensing effect on cosmic microwave background polarization, Phys. Rev. D **58,** 023003 (1998).

[32] K. Kohri and T. Terada, Semianalytic calculation of gravitational wave spectrum nonlinearly induced from primordial curvature perturbations, Phys. Rev. D **97,** 123532 (2018).

[33] T. Fujita, S. Kuroyanagi, S. Mizuno, and S. Mukohyama, Blue-tilted primordial gravitational waves from massive gravity, Phys. Lett. B **789,** 215 (2019).

[34] S. A. Sanidas, R. A. Battye, and B. W. Stappers, Constraints on cosmic string tension imposed by the limit on the stochastic gravitational wave background from the European Pulsar Timing Array, Phys. Rev. D **85,** 122003 (2012).

[35] C. Ringeval and T. Suyama, Stochastic gravitational waves from cosmic string loops in scaling, J. Cosmol. Astropart. Phys. 12 (2017) 027.

[36] J. J. Blanco-Pillado and K. D. Olum, Stochastic gravitational wave background from smoothed cosmic string loops, Phys. Rev. D **96,** 104046 (2017).

[37] N. Kitajima, J. Soda, and Y. Urakawa, Gravitational wave forest from string axiverse, J. Cosmol. Astropart. Phys. 10 (2018) 008.

[38] W. Hu, R. Barkana, and A. Gruzinov, Cold and Fuzzy Dark Matter, Phys. Rev. Lett. **85,** 1158 (2000).

[39] D. J. E. Marsh and J. Silk, A model for halo formation with axion mixed Dark Matter, Mon. Not. R. Astron. Soc. **437,** 2652 (2014).

[40] H.-Y. Schive, T. Chiueh, and T. Broadhurst, Cosmic structure as the quantum interference of a coherent dark wave, Nat. Phys. **10,** 496 (2014).

[41] B. Schwabe, J. C. Niemeyer, and J. F. Engels, Simulations of solitonic core mergers in ultralight axion dark matter cosmologies, Phys. Rev. D **94,** 043513 (2016).

[42] L. Hui, J. P. Ostriker, S. Tremaine, and E. Witten, Ultralight scalars as cosmological dark matter, Phys. Rev. D **95,** 043541 (2017).

[43] R. Saito and J. Yokoyama, Gravitational Wave Background as a Probe of the Primordial Black Hole Abundance, Phys. Rev. Lett. **102,** 161101 (2009).